



# OPEN Chitosan/ferrous oxide nanocomposite for the sunlight-driven photocatalytic degradation of organic azo dye in aqueous solutions and aquaculture effluents wastewater

Ahmed E. Alprol<sup>1</sup>, Ahmed Bakr<sup>2</sup>, Sameerah I. Al-Saeedi<sup>3</sup>, Abdallah Tageldein Mansour<sup>4</sup>✉, Ehab El-Haroun<sup>5</sup>✉, Maymounah N. Alharthi<sup>3</sup> & Mohamed Ashour<sup>1</sup>✉

The current work presents a novel and sustainable approach that uses the synthesized Chitosan/Ferrous Oxide Nanocomposite (CFON) to remove the organic azo dye, Acid Red 73 (AR73), a hazardous pollutant commonly found in industrial wastewater, from aqueous solutions and aquaculture effluents wastewater. The CFON exhibited excellent photocatalytic degradation performance under sunlight irradiation. Batch adsorption experiments were conducted to investigate the influence of various parameters on the removal efficiency of the dye, including pH, contact time, adsorbent dosage, initial concentration, and temperature. The results showed that the nanocomposite effectively achieved a maximum removal percentage of 99.3% under optimal conditions (pH 5 for 180 min at 80 and 100 mg with 75 mg L<sup>-1</sup> and 30 °C). Kinetic studies revealed that the adsorption process followed a pseudo-second-order model, indicating that chemisorption is the dominant mechanism. The impact of different light sources on dye removal efficiency was evaluated, confirming the superior performance of sunlight-driven photocatalysis. The application of CFON to improve water quality in aquaculture was investigated and showed effectively reduced conductivity, total dissolved solids, turbidity, and nitrate levels, demonstrating its potential for sustainable water management. This work highlights the promising potential of CFON as an environmentally friendly and efficient material to remove AR73 and improve aquaculture wastewater quality.

**Keywords** Acid red 73 dye, Adsorption, Chitosan, Ferrous oxide, Nanocomposite, Photocatalysis, Wastewater treatment, Water quality

In recent years, nanotechnology has become a highly versatile field, with nanoparticles (NPs) gaining attention for their unique characteristics and minimal harmful effects<sup>1–3</sup>. Magnetic NPs, particularly iron oxide (Fe<sub>3</sub>O<sub>4</sub>) NPs, are increasingly popular in bioengineering and biomedical applications for their ability to interact at the cellular and molecular level in both in vitro and in vivo settings<sup>4,5</sup>. These NPs are favored for their superparamagnetic properties, biocompatibility, and crystalline structure. Fe<sub>3</sub>O<sub>4</sub> NPs have a crystalline morphology with numerous edges, corners, and potentially reactive sites, making them promising as antibacterial agents<sup>6</sup>. NPs smaller than 100 nm have reliable physical and chemical properties, but to be used in bioengineering environments applications, they must be coated to ensure their safety and stability in biological environments<sup>7,8</sup>.

<sup>1</sup>National Institute of Oceanography and Fisheries (NIOF), Cairo 11516, Egypt. <sup>2</sup>Environment and Bio-agriculture Department, Faculty of Agriculture, Al-Azhar University, Cairo, Egypt. <sup>3</sup>Department of Chemistry, College of Science, Princess Nourah bint Abdulrahman University, P.O. Box 84428, Riyadh 11671, Saudi Arabia. <sup>4</sup>Animal and Fish Production Department, College of Agricultural and Food Sciences, King Faisal University, Al-Ahsa, Saudi Arabia. <sup>5</sup>Department of Integrative Agriculture, College of Agriculture and Veterinary Medicine, United Arab Emirates University, Al Ain, P.O. Box 15551, Abu Dhabi, United Arab Emirates. ✉email: amansour@kfu.edu.sa; ehab.reda@uaeu.ac.ae; microalgae\_egypt@yahoo.com

Chitosan is a biopolymer derived from the deacetylation of chitin<sup>9</sup>. It is a linear polysaccharide with three types of functional groups (amino, primary, and secondary hydroxyl groups) that can be used as a base for combining therapeutics, imaging agents, and targeting ligands<sup>10</sup>. Chitosan exhibits antimicrobial properties against a variety of microbes while being non-toxic to human cells<sup>11–13</sup>. The combination of chitosan and ferrous oxide into a nanocomposite enhances the material's properties for dye removal<sup>14</sup>. The chitosan matrix provides a platform for the dispersion of ferrous oxide nanoparticles, which can act as a photocatalyst under sunlight irradiation<sup>15</sup>. The ferrous oxide nanoparticles (CFON) can absorb sunlight, particularly in the visible and near-infrared regions, and generate reactive oxygen species (ROS) such as hydroxyl radicals ( $\cdot\text{OH}$ ) and superoxide anions ( $\text{O}_2^{\cdot-}$ )<sup>16,17</sup>.

The CFON not only facilitates the photocatalytic degradation of the dye but also offers the advantage of magnetic separation, which simplifies the post-treatment process<sup>18,19</sup>. The magnetic properties of the ferrous oxide allow for easy recovery of the nanocomposite from the treated water using an external magnetic field, which is particularly useful for continuous or large-scale wastewater treatment systems<sup>20,21</sup>. However, several studies reported that pollutants, including pesticides, dyes, and heavy metal ions, damage water supplies, which is one of the biggest environmental issues facing the globe today<sup>22–24</sup>.

Because synthetic dyes are present, the increasing release of industrial effluents, especially from the production of paper, leather, and textiles threatens aquatic habitats<sup>25</sup>. These dyes, which frequently have vivid colors and intricate aromatic compounds, are unable to break down naturally, which causes pollution to remain and has negative effects on aquatic life<sup>26</sup>. AR73 is a widely used azo dye that is highly poisonous and can cause cancer and mutations, which are discrepancies in aquatic organisms' development. The removal of AR73 from wastewater is crucial for environmental protection and water resource management. Several conventional treatment methods have been employed to address dye-laden wastewater, including coagulation-flocculation, membrane filtration, and biological treatments<sup>27–30</sup>. However, these methods often suffer from limitations such as incomplete removal, high operational costs, and the generation of secondary sludge, necessitating the exploration of alternative, more sustainable approaches<sup>31</sup>.

Photocatalysis has emerged as a promising technology for dye removal due to its effectiveness, environmental friendliness, and cost-efficiency. Adsorption utilizes the surface properties of porous materials to bind dye molecules, effectively removing them from the water<sup>32</sup>. While, photocatalysis, on the other hand, employs light-activated catalysts to generate reactive species, such as hydroxyl radicals, which degrade dye molecules into less harmful compounds<sup>3</sup>. As a result, it is an appropriate method of treatment for eliminating dyes from aquatic medium.

Aquaculture effluent refers to the wastewater generated from aquaculture operations, this effluent contains various substances and pollutants that can impact water quality and the surrounding ecosystem if not properly managed<sup>33</sup>. High levels of nutrients in aquaculture effluent can become poisonous to plants and alter their protein synthesis, enzyme activities, photosynthesis, oxidative stress response, membrane permeability, and respiratory processes<sup>34,35</sup>. This aquaculture effluent is considered a global threat to aquatic ecosystems due to its influence on nearby waters and groundwater<sup>36</sup>. These parameters are crucial indicators of the effluent's environmental impact and can affect the health of aquatic organisms and overall water quality. To treat aquaculture effluent, chitosan and  $\text{Fe}_2\text{O}_3$  have been utilized as effective treatment methods. Chitosan, a biopolymer derived from chitin, has exceptional adsorption properties and can effectively remove suspended solids, organic matter, and nutrients from the effluent. It acts as a flocculant and coagulant, aiding in the formation of larger particles that can be easily separated from the water<sup>37</sup>.

Also,  $\text{Fe}_2\text{O}_3$ , known as ferrate, is a powerful oxidizing agent that can effectively degrade organic pollutants and remove nutrients from the water<sup>38</sup>. It can oxidize and break down various contaminants, including suspended solids, ammonia, and organic matter. Additionally,  $\text{Fe}_2\text{O}_3$  has the advantage of being environmentally friendly, as it decomposes into non-toxic byproducts. When chitosan and  $\text{Fe}_2\text{O}_3$  are combined in the treatment of aquaculture effluent, they can synergistically enhance the removal efficiency of pollutants. Chitosan can help in aggregating the suspended solids and organic matter, while  $\text{Fe}_2\text{O}_3$  can oxidize and degrade them. This combined treatment approach can significantly improve water quality and minimize the environmental impact of aquaculture effluent, ensuring the sustainability of aquaculture operations and the protection of surrounding ecosystems<sup>39</sup>.

In recent years, chitosan-based nanocomposites have gained significant attention for wastewater treatment due to their biocompatibility, biodegradability, and high adsorption capacity<sup>40</sup>. Several studies have explored composites such as chitosan- $\text{TiO}_2$ , chitosan- $\text{ZnO}$ <sup>41,42</sup> and chitosan- $\text{Fe}_3\text{O}_4$ , which exhibit effective photocatalytic properties under UV light irradiation. However, these systems often depend on non-renewable energy sources (e.g., artificial UV lamps), limiting their practical applications in low-resource or rural settings as reported by Quy, et al.<sup>42</sup>. Moreover, many of these composites lack the ability to be easily separated and reused, a factor essential for large-scale or continuous treatment operations.

More recently, some researchers such as Arockiaraj et al.<sup>43</sup> investigated chitosan-ferric oxide composites, demonstrating good adsorption capacity for dyes and heavy metals. Yet, the majority of these studies focus on either adsorption only, without integrating photocatalytic mechanisms, or on model/synthetic wastewater matrices rather than real-world effluents. Furthermore, only a limited number of works have addressed their performance under natural sunlight, which is critical for sustainable photocatalysis in environmental applications<sup>44</sup>. In contrast, the present study introduces a Chitosan/Ferrous Oxide Nanocomposite (CFON) that combines the advantages of both materials: the functional groups and adsorption capability of chitosan with the sunlight-responsive photocatalytic activity and magnetic recoverability of  $\text{Fe}_2\text{O}_3$ . This composite was tested not only against synthetic Acid Red 73 dye but also against real aquaculture effluent, demonstrating its efficiency in improving key water quality parameters such as TDS, EC, turbidity, and nitrate levels. To our knowledge, this is among the few studies to investigate the dual-functionality (adsorption and photocatalysis) of a chitosan-iron

oxide composite under natural sunlight conditions and within a real wastewater treatment scenario, representing a practical and scalable approach toward eco-friendly water purification.

Therefore, this study aims to create a CFNO for use as an adsorption material to remove AR73 dye from water under sunlight exposure photocatalysis. Various parameters such as initial dye concentration, pH, contact time, column bed heights, temperature, and adsorbent dose were evaluated. The catalytic activity of the nanocomposite in degrading the dye under different light conditions was also examined. The potential of the nanocomposite for improving water quality in aquaculture applications was assessed. Changes in the physical, chemical, and morphological structure due to reaction were studied through zeta potential, Fourier Transform Infrared Spectroscopy (FTIR), Energy-Dispersive X-ray Spectroscopy (EDX), and Scanning Electron Microscopy (SEM) characterizations. Thermodynamic and kinetics studies were conducted, and various sorption isotherm models were used to analyze the adsorption mechanism. Moreover, the impact of CFNO on improving the water quality parameters of rearing aquaculture effluent was investigated.

## Materials and methods

### Adsorbent stock solution

The preparation of AR73 stock solution was prepared by dissolving one gram of AR73 powder in 1000 ml of water, to get the desired concentration of  $1000 \text{ mg L}^{-1}$ . The chemical structure of AR73 is  $\text{C}_{22}\text{H}_{14}\text{N}_4\text{Na}_2\text{O}_7\text{S}_2$  (Supplementary Fig. 1).

### Instruments

FTIR spectra of the powder sample were obtained using a Bruker IFS 66v/S spectrometer from Germany and an IR Affinity – 1 S-SHIMADZU spectrometer from Kyoto, Japan. Attenuated total reflection (ATR) was utilized for recording FTIR spectra, with 32 scans in the spectral range of  $4000 - 400 \text{ 1/cm}$  and a resolution of  $4 \text{ cm}^{-1}$ . The composite material composed of adsorbent was further analyzed for shape and elemental content using SEM and EDX with the JEOL JSM-IT200 instrument at a magnification of  $\times 40,000$ . Zeta potential measurements were conducted with a HORIBA Scientific SZ-100 nanoparticle analyzer from the UK.

### Experimental methods

#### *Preparation of chitosan/ferrous oxide nanocomposite (CFON)*

To prepare the CFON, 2 g of nano-chitosan was dissolved in 100 mL of a 2% acetic acid solution. Once the nano-chitosan was completely dissolved, 2 mL of distilled water was added and the mixture was shaken well for 2 h at  $60^\circ\text{C}$ . Next, a 0.1 M solution of NaOH was added drop by drop until a slightly alkaline solution was achieved and then left to gel for 48 h. The resulting gel was washed with demineralized water until neutral. Subsequently, 50 mL of  $\text{Fe}_2\text{O}_3$  solution was mixed and stirred at  $60^\circ\text{C}$  for 60 min. Following this, 50 mL of chitosan solution was added to the mixture and continuously stirred at  $60^\circ\text{C}$  for 2 h. The mixture was then slowly added to 2 mL of a 2.5% glutaraldehyde solution, which acted as the cross-linking agent and catalyst, and stirred for an additional 15 min. The hydrogel was dried overnight in an oven at  $80^\circ\text{C}$  until all water content had evaporated, resulting in the final product<sup>45</sup>.

#### *Adsorption experiments*

The method used for the pH study was to maintain the initial pH values between 3 and 10 before adding the adsorbent to 50 mL of AR73 solution containing 40 mg of the CFON dose in conical flasks. For three hours at room temperature, each sample was agitated with a mechanical shaker while exposed to Ultraviolet (UV) light. Using a digital pH meter, the equilibrium pH was measured. To guarantee maximum adsorption, the initial pH value at which maximum adsorption occurred at equilibrium was changed for subsequent research.

A kinetic experiment<sup>46</sup> was conducted to investigate the adsorption of AR73 onto the CFON. The initial concentration of AR73 was set at  $60 \text{ mg L}^{-1}$  and the adsorbent dosage was 40 mg. Throughout the experiment, the pH was kept constant at pH 3, and different contact times varied from 15, 30, 45, 60, 120, and 180 min. After that, the mixture was shaken mechanically under UV-irradiation conditions at room temperature. After a predetermined amount of time, the sample from each flask was filtered, and the concentration of AR73 was measured. To find AR73's adsorption capability at a specific time (t), calculations were done. Also, the pseudo-first-order (PFO), pseudo-second-order (PSO), and Interparticle diffusion kinetic models were fitted to the experimental data to have a better understanding of the adsorption mechanism.

To investigate the influence of CFON dosage on AR73 removals under UV-irradiation conditions and dark conditions. Prepare a 60 ppm AR73 solution using distilled water. Adjust the pH to 3. Then prepare a series of identical containers (beakers) with 50 mL of the dye solution each. Add different amounts of the nanocomposite to each container (20, 40, 60, 80, and 100 mg). Place half of the containers with varying nanocomposite dosages under the UV lamp and dark conditions at room temperature and 200 rpm. Ensure consistent distance and exposure for all samples. Place the other half of the containers in a dark chamber for 3 h to serve as the control group.

To compare the effect of initial dye concentration on removal by CFON under sunlight and dark conditions: Prepare a series of AR73 solutions with varying initial concentrations (25, 50, 75, 100, and 200 ppm) using distilled water. Adjust the pH of each solution to 3 using the pH buffer. Add a fixed amount (40 mg) of the CFON to a set of identical containers (e.g., beakers or flasks). Place half of the flasks with the dye solutions and CFON under direct sunlight for 3 h. Avoid shaking to maintain consistent light exposure. The other half of the containers in a dark chamber for 3 h to serve as the control group with shaking at 200 rpm.

To compare the batch and the fixed column, an experiment was added to investigate the effect of different bed heights of CFON, on the removal of AR73 dye has been investigated using a fixed bed column setup. The experiment was performed under varying bed heights of columns: 1 cm, 1.5 cm, 2 cm, and 2.5 cm, while

maintaining initial dye concentration ( $50 \text{ mg L}^{-1}$ ), time (3 h), temperature of  $30^\circ\text{C}$ , and pH constant (pH 5). After the exposure period, separate the adsorbent from the dye solutions using filtration or centrifugation. Analyze the dye concentration in the treated solutions using a UV-Vis spectrophotometer. Then calculate the percentage removal and adsorption capacity ( $q_e$ ) for each dye concentration under both sunlight and dark conditions. The concentration of AR73 dye was measured using spectrophotometry  $\lambda_{\text{max}} = 510 \text{ nm}$ . The percentage removal and adsorption capacities ( $q_e$ ) were estimated using Eqs. (1,2):

$$\text{AR73 Removal (\%)} = \frac{(C_i - C_f)}{C_i} \times 100 \quad (1)$$

$$q_e = \frac{(C_i - C_f) \times V}{W} \quad (2)$$

where: the concentration is represented by the symbols  $C_i$  and  $C_f$  are the liquid-phase concentrations of AR73 dye in  $\text{mg L}^{-1}$  at initial and equilibrium, respectively. In contrast,  $q_e$  is the maximal adsorption at monolayer ( $\text{mg g}^{-1}$ ). The mass of the adsorbent is ( $W$ ) with gram and the volume of the solution is  $V$  (L).

#### *Aquaculture effluents wastewater treatment*

Correspondingly, the impacts of CFON on water quality parameters of aquaculture effluent were assessed. A real aquaculture effluent sample was collected from a private fish farm in Alexandria, Egypt ( $31^\circ 12' 30.07'' \text{ N}$ ,  $29^\circ 58' 41.66'' \text{ E}$ ), where Nile tilapia (*Oreochromis niloticus*) is cultivated. The water quality parameters were analyzed before and after CFON treatment. The following methodologies were employed: Dissolved Oxygen (DO), Electrical Conductivity (EC), Total Dissolved Solids (TDS), and Turbidity were measured using a Multiparameter system (HI9829 digital pro). Nitrate ( $\text{NO}_3^-$ ) concentrations were determined according to standard methods<sup>47</sup> and the values after treatment with CFON compared to the same values before treatment. pH variations were monitored to assess potential shifts due to chitosan alkalinity. For ammonia removal assessment, additional ammonia was introduced to the effluent sample to reach a concentration of  $10 \text{ mg L}^{-1}$ . The treated water was subsequently filtered to remove suspended particulates and precipitates. A control experiment using deionized water with an equivalent ammonia concentration was conducted to evaluate the adsorption efficiency of CFON under identical conditions. CFON was synthesized and applied as an adsorbent for water quality improvement. The CFON was introduced into the aquaculture effluent under controlled conditions to evaluate its efficacy in contaminant removal. The treatment was conducted at an optimal pH of 8.0, with a contact time of 120 min and an adsorbent dosage of  $0.1 \text{ g } 100 \text{ mL}^{-1}$  of wastewater. The impact of CFON treatment was assessed based on the percentage reduction of key water quality parameters. Given the relatively low initial ammonia concentration in the effluent sample, a controlled amount of ammonia solution was introduced to achieve a final concentration of  $10 \text{ mg L}^{-1}$ , ensuring a more precise assessment of the adsorbent's removal capacity. Following the adsorption process, the treated effluent was subjected to filtration to eliminate precipitates and suspended particles, thereby enhancing water clarity and purity. A control experiment was simultaneously conducted using deionized water with an equivalent ammonia concentration to distinguish between adsorption efficiency and potential background interferences.

## Results and discussion

### Characterization of adsorbent nanocomposite

Supplementary Fig. 2 shows the characterization of CFON adsorbent. Zeta potential ( $\zeta$ ) is a measure of the electrostatic potential difference between a colloid (nanocomposite particle) and the surrounding dispersing medium (aqueous solution). The data presented in Supplementary Fig. 2A provides valuable information on the surface charge characteristics of the CFON and its potential interaction with AR73 dye. The result displays an average zeta potential of  $28.8 \text{ mV}$ , indicating a moderately positive surface charge on the chitosan/ferrous oxide nanocomposite. This positivity is attributed to the presence of protonated amino groups ( $\text{NH}_3^+$ ) in chitosan under slightly acidic or neutral pH conditions<sup>48</sup>. Peak 1 represents the majority of nanoparticles with a zeta potential of  $28.9 \text{ mV}$ , consistent with the average value. The high peak area (99.8%) suggests that most particles possess this positive surface charge. Peak 2, with a value of  $-6.36 \text{ mV}$  and a small area (0.2%), indicates a minor population of negatively charged particles, possibly due to variations in surface composition or iron oxide distribution. Peak 3 at  $0 \text{ mV}$  signifies a negligible population of electrically neutral particles. As AR73 is an anionic dye, carrying a negative charge, the positive surface charge of the CFON can attract the dye molecules, enhancing the adsorption process and facilitating the removal of the dye from the aqueous solution. The moderately positive zeta potential of the CFON suggests favorable electrostatic interactions for AR73 adsorption, supported by the dominant population of positively charged particles (Peak 1)<sup>49</sup>. However, the presence of a minor negatively charged population (Peak 2) indicates a potential for the repulsion of dye molecules. Further investigation could investigate the impact of pH on zeta potential, as chitosan's surface charge may vary with the acidity or alkalinity of the solution, potentially affecting the efficiency of AR73 dye adsorption.

FTIR spectroscopy serves as an indispensable tool in analytical chemistry, facilitating the identification of functional groups within molecules through the absorption of infrared radiation at varying wavelengths. The FTIR analysis of the CFON utilized for AR73 adsorption is depicted in Supplementary Tables 1 and Supplementary Fig. 2B. The broad absorption peak at  $3419.476 \text{ cm}^{-1}$ , attributed to the O-H-NH stretch, signifies the presence of hydroxyl and amine groups, likely originating from the polysaccharide structure of chitosan and potentially adsorbed water molecules. These hydroxyl groups play a pivotal role in facilitating hydrogen bonding with dye molecules, thus influencing the adsorption process significantly. Also, this band underscores their significance in facilitating hydrogen bonding interactions with dye molecules. Hydrogen bonding is



a fundamental phenomenon in adsorption processes, wherein the attractive forces between polar functional groups on the adsorbent surface and the dye molecules play a crucial role in the adsorption mechanism.

The appearance of a peak at  $2076.421\text{ cm}^{-1}$  suggests the presence of carbonyl groups (C=O stretch), possibly arising from aldehydes or ketones. The impact of these groups on dye adsorption hinges upon the specific functional groups present in the AR73 molecule, potentially involving dipole-dipole interactions or hydrogen bonding with the dye. Additionally, the detection of carbon-carbon double bonds (C=C stretch) at  $1637.312\text{ cm}^{-1}$  implies their existence in aromatic rings or alkenes within the chitosan structure. These double bonds can engage in pi-pi interactions with the aromatic rings commonly found in dye molecules, thereby augmenting adsorption. In addition, the presence of amine groups (C-N stretch) is indicated by a peak at  $1399.741\text{ cm}^{-1}$ , suggesting potential interactions with specific functional groups within the AR73 dye molecule, such as carboxylic acid or sulfonic acid groups, through electrostatic interactions or hydrogen bonding.

Moreover, the presence of C-O bonds, likely originating from alcohol or ether groups in the chitosan structure, is indicated by a peak at  $1104.428\text{ cm}^{-1}$ . Analogous to the O-H stretch, these groups can engage in hydrogen bonding with dye molecules. The detection of the Fe-O bond at  $642.691\text{ cm}^{-1}$  confirms the presence of iron oxide in the nanocomposite. Although not directly involved in dye binding, the Fe-O bond contributes to the nanocomposite's surface properties, influencing its surface charge, porosity, and ultimately, its adsorption capacity. Also, the characteristic peaks observed at approximately  $410$  to  $565\text{ cm}^{-1}$  correspond to octahedral-metal stretching ( $\text{Fe}_2\text{O}_3$ ). The FTIR analysis indicates the presence of a substantial amount of phenolic acids, carboxylic acids, and amines. The detection of free hydroxyl groups (–OH), phenolic (–CHOH) carboxylic (–COOH) acids, and other functional groups such as amine (–NH<sub>2</sub>), may be attributed to the chitosan polymer.

While, the data gathered from SEM analysis in Supplementary Fig. 1C can be utilized to enhance the production process of CFON and customize their characteristics for specific uses, like removing AR73 dyes from water solutions. SEM analysis is a commonly used method for examining nanomaterials and nanostructures due to its ability to provide detailed images of a sample's surface features, composition, and size. The SEM image indicates that the nanocomposite has an irregular surface morphology, with particles appearing clustered or dispersed. The particle size in the nanocomposite ranges from  $13.07\text{ nm}$  to  $19.88\text{ nm}$ , falling within the nanoparticle size range. This rough surface morphology may be advantageous for applications requiring a large surface area, such as adsorption. EDX is a technique that combines with SEM to analyze the elemental composition of a sample. When an electron beam interacts with the sample, it causes the atoms to emit X-rays with specific energies. By studying the energy and intensity of these X-rays, the elements present in the sample can be identified. EDX provides information about the elements and their relative abundance in a specific area of the sample. Supplementary Tables 2 and Supplementary Fig. 2D display the elemental composition of the CFON obtained through EDX analysis.

The highest mass percentage (39.78%) is carbon, which is expected due to the carbon-rich nature of chitosan. Oxygen accounts for the second highest percentage (43.49%), found in both chitosan and ferrous oxide (FeO). The presence of chlorine (10.15%) may be attributed to chloride salts used in the synthesis process. The detection of iron (0.46%) confirms the presence of ferrous oxide nanoparticles in the chitosan matrix, although the low iron content suggests a lower concentration compared to chitosan. The significant presence of carbon, nitrogen, and oxygen indicates the successful integration of chitosan into the nanocomposite. The relatively low iron content implies a higher ratio of chitosan to ferrous oxide. The diverse elements on the surface create a complex chemical environment, potentially beneficial for dye adsorption by providing multiple interaction sites for dye molecules.

## Adsorption experiments

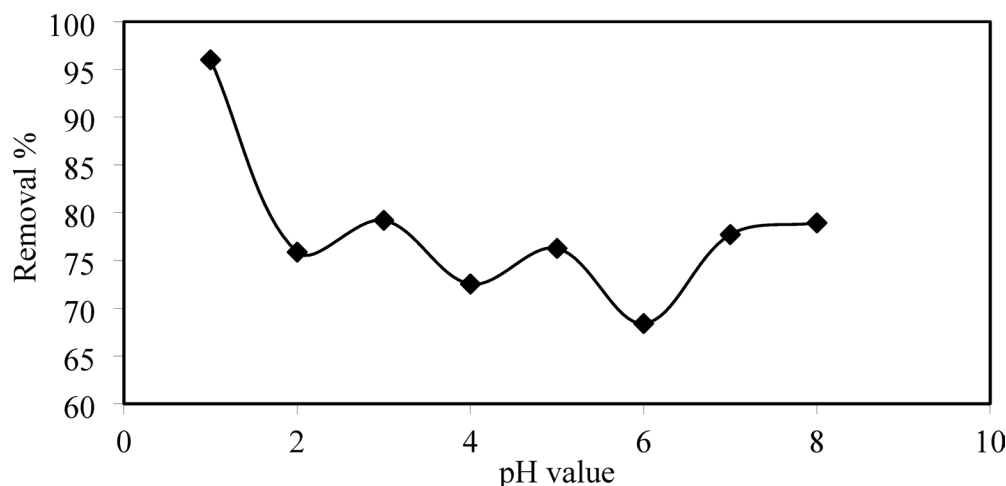
### pH

Figure 1 shows the influence of pH on AR73 removal efficiency by the CFON. The data demonstrates that the removal efficiency of AR73 dye by the CFON adsorbent is generally high across a wide pH range (3–10), with removal percentages exceeding 86% in all cases (Fig. 1). However, there are some fluctuations observed within this range. The highest removal percentage (99.05%) occurs at pH 5, while the lowest (86.34%) is observed at pH 8. The peak removal efficiency at pH 5 suggests an optimal electrostatic interaction between the adsorbent and the dye molecules at this specific pH.

This could be due to a favorable combination of surface charge on the adsorbent and ionization state of the dye, leading to strong attraction. Whereas, the decreased removal efficiency at pH 8 could indicate less favorable electrostatic interactions or changes in the adsorbent's surface properties at this pH, reducing its affinity for the dye molecules<sup>50</sup>. The adsorbent's effectiveness across a broad pH spectrum is a significant advantage, indicating its potential applicability in diverse wastewater treatment scenarios where pH control might be challenging. The observed fluctuations in removal efficiency suggest that pH influences the adsorption process. This is likely due to the impact of pH on both the surface charge of the adsorbent and the ionization state of the dye molecules<sup>51</sup>. The CFON likely has pH-dependent surface charge properties. Zeta potential analysis and changes in pH can alter the protonation/deprotonation of functional groups on the adsorbent surface, thereby affecting the electrostatic interactions between the adsorbent and the dye molecules<sup>52</sup>.

### Contact time

Figure 2 shows the effect of contact time on AR73 removal efficiency by CFON. In the adsorption process, the contact time between the adsorbent and the dye solution plays a crucial role in determining the removal efficiency. It influences the rate at which dye molecules interact with the adsorbent surface and reach equilibrium. Understanding the effect of contact time is essential for optimizing the treatment process and ensuring efficient dye removal (Fig. 2). The data demonstrates a clear trend: as the contact time increases, the percentage removal of AR73 dye and the adsorption capacity ( $q_t$ ) both increase. This indicates that longer contact times allow for more



**Fig. 1.** Influence of pH on removal of AR73 by the CFON.

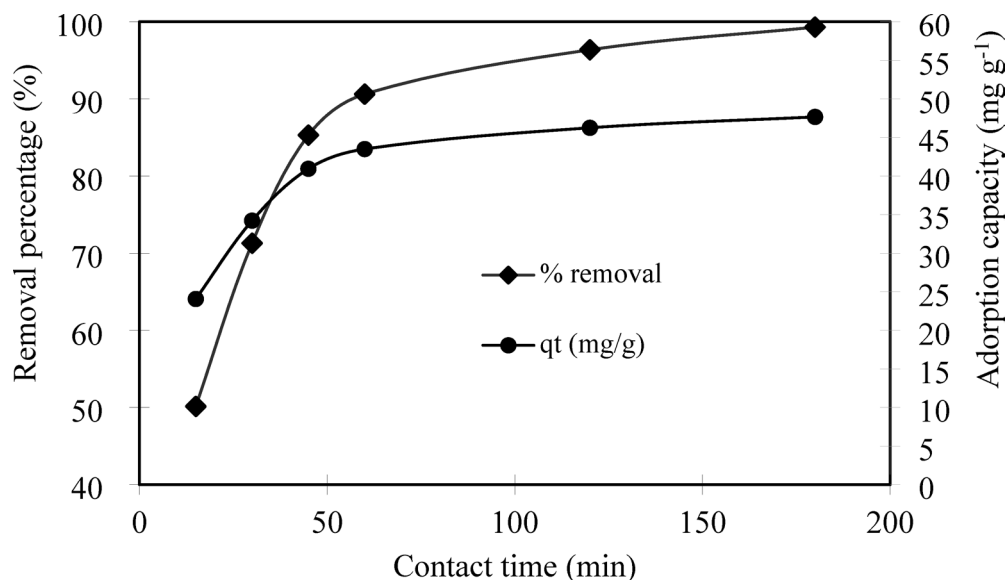


**Fig. 2.** Effect of contact time of AR 73 dye removal efficiency by CFON.

dye molecules to interact with the adsorbent surface and undergo photocatalytic degradation. The removal rate is initially rapid, with a significant increase in percentage removal and  $q_t$  within the first 60 min<sup>53</sup>. This suggests that a large number of readily accessible adsorption sites are available on the adsorbent surface, facilitating fast dye uptake and degradation<sup>54</sup>. While, as the contact time extends beyond 60 min, the rate of removal gradually slows down as the adsorption sites become increasingly occupied and the concentration of dye molecules in the solution decreases. At 180 min, a near-complete removal of the dye (99.3%) is achieved, indicating that the system approaches equilibrium, where the rate of adsorption and degradation balances the rate of desorption. Peng et al. suggest that the adsorption process is primarily influenced by the porous structure of adsorbents, resulting in a slow diffusion of adsorbates through the pores<sup>55</sup>. The photocatalytic degradation of AR 73 dye using Chitosan-iron oxide hybrid composite under UV light likely involves a combination of adsorption and photodegradation processes.

Suggested possible mechanism by: the dye molecules are initially adsorbed onto the surface of the chitosan-iron oxide composite through various mechanisms, as previously discussed (electrostatic attraction, hydrogen bonding, Van der Waals forces). The iron oxide component of the composite absorbs UV light, exciting electrons from the valence band to the conduction band and creating electron-hole pairs. The excited electrons and holes migrate to the surface of the composite. The holes can react with water molecules or hydroxyl ions to generate highly reactive hydroxyl radicals ( $\cdot\text{OH}$ ). Also, the hydroxyl radicals attack the adsorbed dye molecules, breaking them down into smaller, less harmful compounds through oxidation reactions<sup>7</sup>. Finally, the contact time between the Chitosan-iron oxide hybrid composite and the AR73 dye solution significantly impacts the

photocatalytic degradation process. Longer contact times lead to higher removal percentages and adsorption capacities, allowing for near-complete dye removal as the system approaches equilibrium.

#### Adsorbent dosage

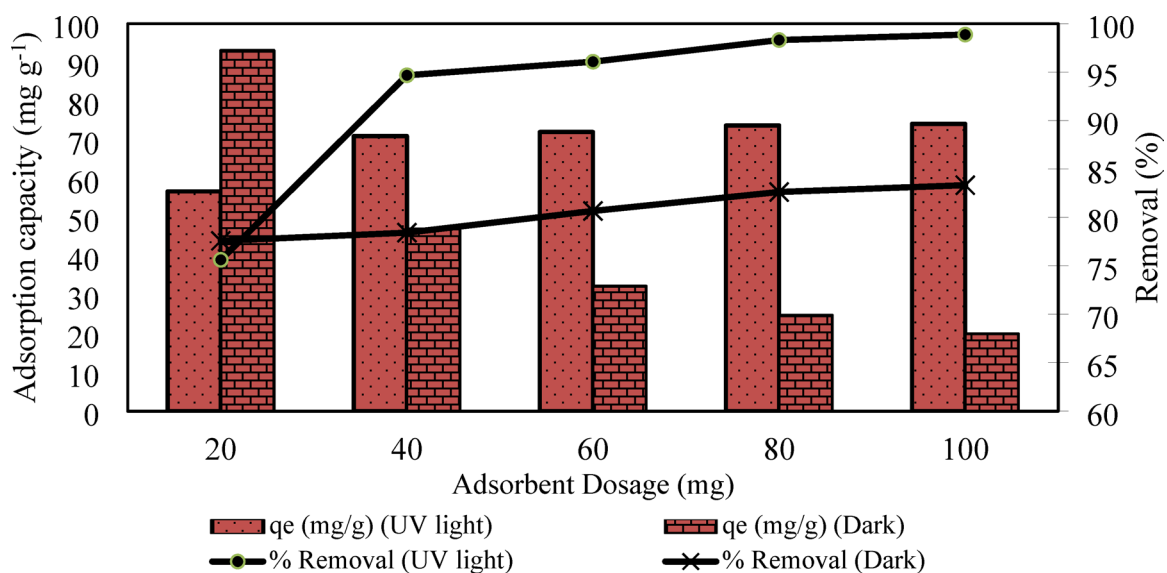
The provided data for a comparison of AR73 dye removal efficiency by CFON under UV light exposure and in dark conditions is presented in Fig. 3. The data clearly shows that exposure to UV light significantly enhances the percentage removal of AR73 compared to dark conditions specialty at higher dosages at 80 and 100 mg. This confirms the photocatalytic activity of the Chitosan/ferrous oxide nanocomposite, where UV light plays a crucial role in generating reactive species that degrade the dye molecules. Interestingly, the adsorption capacity ( $q_e$ ) under dark conditions is higher at lower adsorbent doses ( $93 \text{ mg g}^{-1}$ ) compared to UV conditions<sup>56</sup>. However, as the dose increases, the  $q_e$  values in dark conditions decrease significantly, while they remain relatively stable under UV conditions. As explained earlier, UV light excites the iron oxide component of the composite, leading to the generation of hydroxyl radicals that degrade the dye molecules. This process significantly enhances the overall dye removal efficiency under UV light compared to dark conditions<sup>57</sup>.

In the absence of UV light, dye removal occurs primarily through adsorption processes. The higher  $q_e$  values at lower doses in dark conditions suggest that the available adsorption sites are more effectively utilized when the dye molecule concentration is relatively high compared to the available sites. As the adsorbent dose increases, the number of available adsorption sites becomes much larger than the number of dye molecules in the solution. This leads to a lower utilization of the available sites, resulting in a decrease in  $q_e$  values under dark conditions. Under UV conditions, however, the continuous degradation of dye molecules by the generated radicals allows for sustained adsorption and higher  $q_e$  values even at higher adsorbent doses<sup>58</sup>. The latter could promote dye sorption and boost the production of radicals, which could raise the efficiency of degradation. Many parameters, including surface morphology, bandgaps, sizes, crystallinity, shape, and concentration, affect a nanocatalyst photocatalytic activity<sup>59</sup>.

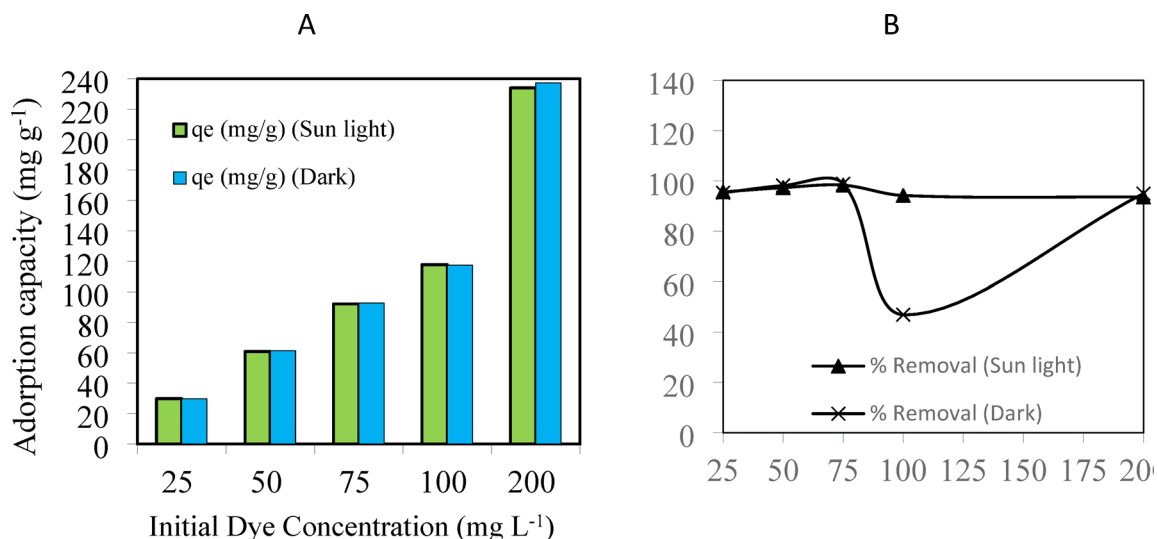
#### Initial AR73 concentration

Figure 4 shows the effect of the initial AR73 dye concentration on its removal by a CFON under sunlight and dark conditions. The data reveals an interesting trend in the removal of AR 73 dye by the CFON as the initial dye concentration increases. While the percentage removal initially increases with increasing dye concentration up to  $75 \text{ mg L}^{-1}$  (reaching 98.319%), it then slightly decreases as the concentration continues to rise to  $200 \text{ mg L}^{-1}$ . In contrast, the adsorption capacity ( $q_e$ ) exhibits a continuous increase with rising initial dye concentration, reaching a maximum of  $234.03 \text{ mg g}^{-1}$  at  $200 \text{ mg L}^{-1}$ .

Sunlight exposure significantly enhances dye removal compared to dark conditions, especially at higher initial concentrations (100 and  $200 \text{ mg L}^{-1}$ ). This suggests a photocatalytic degradation mechanism where sunlight activates the nanocomposite, promoting dye breakdown<sup>60</sup>. In both conditions, the removal efficiency initially increases with increasing dye concentration, reaching a peak, and then slightly declining or plateauing<sup>54</sup>. This behavior can be attributed to the availability of active sites on the nanocomposite. At low concentrations, sufficient sites are available for dye adsorption and degradation. However, as the concentration rises, the sites become saturated, leading to a decrease in removal efficiency<sup>61</sup>. The choice between sunlight and dark conditions depends on the specific application and available resources. While sunlight offers a sustainable and cost-effective approach, achieving consistent results might be challenging due to weather fluctuations. Dark conditions with artificial UV light sources provide more control but require energy input<sup>56</sup>. Chitosan, with its amino and hydroxyl functional groups, provides active sites for dye adsorption through electrostatic interactions



**Fig. 3.** Effect of adsorbent dosage on AR73 removal efficiency under UV light and dark conditions.



**Fig. 4.** Effect of initial AR73 concentration on AR73 removal efficiency under sunlight and dark conditions (A) adsorption capacity (mg g<sup>-1</sup>) and (B) percentage removal %.

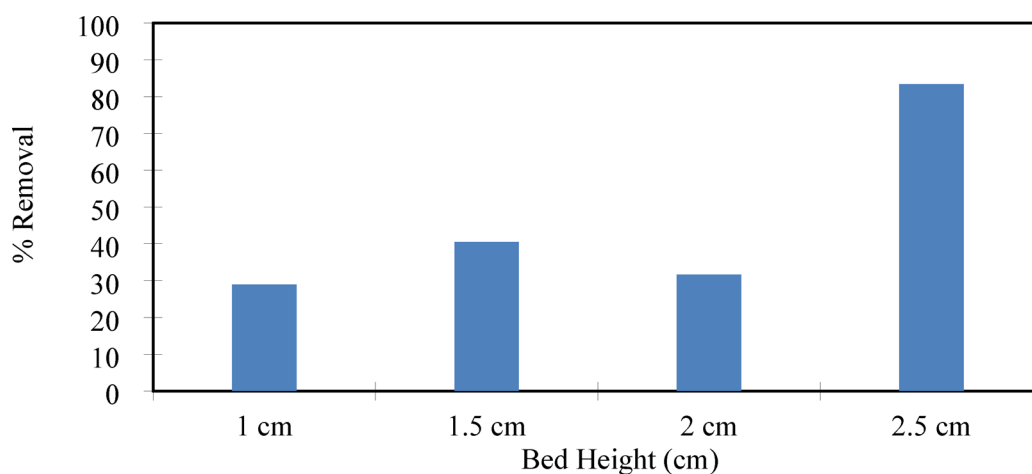


**Fig. 5.** Removal percentages (%) of AR73 dye at different heights of bed using CFON in a fixed bed column setup (the initial dye concentration of 50 mg L<sup>-1</sup> and a pH of 5).

and hydrogen bonding<sup>45</sup>. In addition, ferrous oxide, under sunlight, generates electron-hole pairs. These reactive species interact with water molecules to produce hydroxyl radicals, which are potent oxidizing agents capable of breaking down the dye molecules into smaller, less harmful compounds. Xiao, et al.<sup>62</sup> reported that the general idea behind semiconductor nanomaterials-based photocatalysis is the degradation of organic dye molecules that are derived from ROS, such as superoxide ( $-O_2^-$ ) and hydroxyl ( $-OH$ ). These radicals are created when photogenerated electron holes react with dissolved oxygen ( $O_2$ ) in water, and they function as strong, nonselective oxidants to break down dye pollutants into  $CO_2$  and  $H_2O$ .

#### *Different column bed heights of a nanocatalyst*

The effect of different bed heights of a nanocatalyst, specifically Chitosan/Ferrous Oxide Nanocomposite, on the removal of AR73 dye has been investigated using a fixed bed column setup. Figure 5 presents the percentage removal of the dye under varying bed heights: 1 cm, 1.5 cm, 2 cm, and 2.5 cm while maintaining the initial dye concentration, temperature, and pH constant.

In the experiment, it is observed that the percentage removal of AR73 dye varies with different bed heights. The results showed that at a bed height of 1 cm, the percentage removal is measured at 28.992%. This relatively lower removal efficiency might be attributed to the limited surface area available for adsorption within the smaller bed height. Thus, the contact between the dye molecules and the adsorbent might not be optimal, leading to lower removal rates<sup>63</sup>. As the bed height increases to 1.5 cm, a significant improvement in the removal efficiency is observed, with a percentage removal of 40.476%. This suggests that increasing the bed height provides additional surface area for adsorption, allowing more dye molecules to come into contact with the adsorbent<sup>64</sup>. As a result,



the adsorption capacity is enhanced, leading to higher removal efficiency. However, at a bed height of 2 cm, there is a slight decrease in the percentage removal to 31.653%. This could be due to factors such as channeling or uneven distribution of flow within the column at this particular bed height, which may reduce the effective contact between the dye molecules and the adsorbent. While, at a higher bed height of 2.5 cm, the removal efficiency increases again to 35.294%. This suggests that despite the slight decrease observed at 2 cm, further increasing the bed height still provides additional surface area for adsorption, leading to improved removal efficiency. The observed tendency in the experiment is consistent with the adsorption mechanism and previous studies. Increasing the bed height indeed provides extra surface area for the adsorption process, allowing more dye molecules to be adsorbed onto the CFON. Additionally, the increased bed height results in a longer contact time between the dye molecules and the adsorbent, further enhancing the removal efficiency<sup>65</sup>.

### Photocatalytic activity and AR73 removal mechanism

The photocatalytic activity of a nanocatalyst, such as CFON, in the degradation of AR73 dye can be significantly influenced by different light irradiation conditions. Figure 6 presents the percentage removal of the dye under various light conditions such as dark, UV light, room temperature light, and sunlight. In dark conditions, where light is absent, the photocatalytic activity is minimal, resulting in only 12.605% removal of the dye.

This indicates that light is essential for initiating the photocatalytic degradation process. Under UV light irradiation, there is a slight improvement in the degradation efficiency compared to dark conditions, with a removal rate of 22.829%. UV light provides the necessary energy to activate the nanocatalyst, thereby enhancing its photocatalytic activity<sup>66</sup>. However, the efficiency is still relatively low compared to other light sources. While, room temperature light, such as that from a lead lamp, leads to a further increase in the degradation efficiency, with a removal rate of 28.852%. This suggests that visible light plays a significant role in promoting the photocatalytic degradation process compared to UV light, likely due to its higher energy and broader wavelength spectrum. The most significant improvement in dye removal is observed under sunlight irradiation, where a removal rate of 42.437% is achieved. The visible light in sunlight, which is part of a wide spectrum, effectively activates the nanocatalyst and encourages the dye molecules to break down<sup>66</sup>. Additionally, sunlight provides a higher intensity of light compared to artificial light sources, further enhancing the photocatalytic activity. Some factors that can change how well the nanocatalyst works include: brighter light can make the nanocatalyst work faster, and sunlight can make more types of nanocatalyst work better<sup>67</sup>. Also, using more nanocatalyst can make the dye disappear faster. But if we use too much, it won't work as well. The type of liquid we use can also change how well the nanocatalyst works, depending on whether it's more acidic or basic. The role of sunlight in photocatalysis for AR73 removal is diverse: Sunlight is essential for providing the energy needed to activate the photocatalyst process. When the photocatalyst absorbs photons from sunlight, it creates electron-hole pairs. Sunlight's wide spectrum, which includes UV and visible light, allows for the targeted activation of photocatalysts with varying bandgap energies. This is crucial for developing visible-light-responsive photocatalysts that can broaden the scope of photocatalysis beyond UV light limitations. By using sunlight as the primary energy source for photocatalysis, it adheres to green chemistry principles by eliminating the need for additional energy input and reducing the environmental impact associated with traditional wastewater treatment methods. Sunlight is a readily available, renewable resource that is cost-effective for large-scale applications, particularly in regions with ample sunlight. This makes sunlight photocatalysis a financially feasible option<sup>68</sup>.

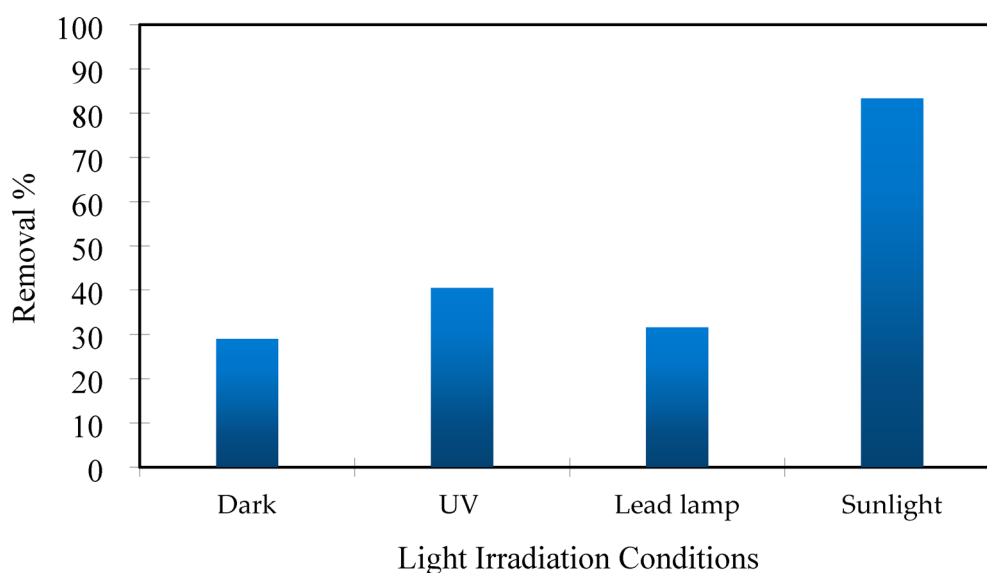
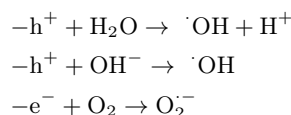


**Fig. 6.** Removal percentages (%) of AR73 under various light irradiation conditions (dark, UV, lead lamps, and sunlight) using CFON (at a dosage of 10 mg/mL, AR73 concentration of 25 mgL<sup>-1</sup>, and pH 3 without shaking for 180 min).

Upon exposure to sunlight, the  $\text{Fe}_2\text{O}_3$  nanoparticles embedded in the CFON matrix act as semiconductors with a relatively narrow bandgap ( $\sim 2.1$  eV), which allows them to absorb visible light<sup>69</sup>. The absorbed photons excite electrons ( $e^-$ ) from the valence band (VB) to the conduction band (CB), leaving behind positively charged holes ( $h^+$ ) in the VB. These photogenerated charge carriers play a central role in generating reactive oxygen species (ROS) via the following reactions<sup>69</sup>:



These ROS particularly hydroxyl radicals ( $\cdot\text{OH}$ ) are highly reactive and non-selective, and they oxidize the dye molecules by attacking their aromatic rings, azo bonds ( $-\text{N}=\text{N}-$ ), and sulfonic groups, eventually breaking them down into intermediate compounds and ultimately mineralizing them into  $\text{CO}_2$ ,  $\text{H}_2\text{O}$ , and inorganic ions. The combined action of adsorption (by chitosan) and ROS-induced oxidation (by  $\text{Fe}_2\text{O}_3$  under sunlight) provides a dual degradation pathway for AR73 dye removal, enhancing overall treatment efficiency. This synergy is especially effective under natural sunlight, which offers a broad wavelength spectrum to trigger ROS formation efficiently. The enhanced removal under sunlight, compared to dark or UV-only conditions, strongly supports the proposed ROS-driven mechanism.

### Impact of temperature on AR73 removal and thermodynamic parameters

The data in Fig. 7 indicates that the removal efficiency of AR73 dye by the CFON decreases with increasing temperature. This behavior suggests an exothermic nature of the adsorption process, meaning the adsorption is favored at lower temperatures. As the temperature increases, the kinetic energy of both the dye molecules and the adsorbent material increases. This leads to increased mobility of dye molecules, then higher kinetic energy allows dye molecules to move more freely, reducing the likelihood of them interacting with and being adsorbed onto the nanocomposite surface. The thermodynamic parameters in Supplementary Table 3 showed the positive value of enthalpy change ( $\Delta H^\circ$ ) ( $56.99 \text{ kJ mol}^{-1}$ ) confirming the exothermic nature of the adsorption process. This means the adsorption process releases heat, making lower temperatures more favorable. The negative value of entropy change ( $\Delta S^\circ$ ) ( $-0.154 \text{ J mol}^{-1} \text{ K}^{-1}$ ) suggests a decrease in randomness at the solid/liquid interface during adsorption. This could be due to the ordered arrangement of dye molecules on the adsorbent surface<sup>70</sup>. The negative values of Gibbs free energy change ( $\Delta G^\circ < -10 \text{ kJ mol}^{-1}$ ) indicate that the adsorption process is spontaneous at all temperatures investigated. This means the adsorption process is thermodynamically favorable. The constant value of  $\Delta G^\circ$  across the temperature range suggests that the driving force for adsorption remains consistent despite the changing temperature<sup>71</sup>. The negative value of  $\Delta G^\circ$  ( $< -10 \text{ kJ mol}^{-1}$ ) suggests that the dominant mechanism is physical adsorption, involving weak forces of attraction like van der Waals forces, hydrogen bonding, and electrostatic interactions. This mechanism is further supported by the positive  $\Delta H^\circ$  value, indicating that the adsorption process is driven by the release of heat<sup>72</sup>.

### Analysis of sorption isotherms for AR73 dye removal

The adsorption behavior of AR73 onto a CFON was investigated by using three isotherm models: Freundlich<sup>73</sup>, Langmuir<sup>74</sup>, and Harkins-Jura<sup>75</sup>. The equations can be found in the Supplementary Table 4. The data from the adsorption experiments were fitted to the linear forms of these models, and the resulting parameters are presented in Table 1. The Freundlich model describes multilayer adsorption on heterogeneous surfaces. The

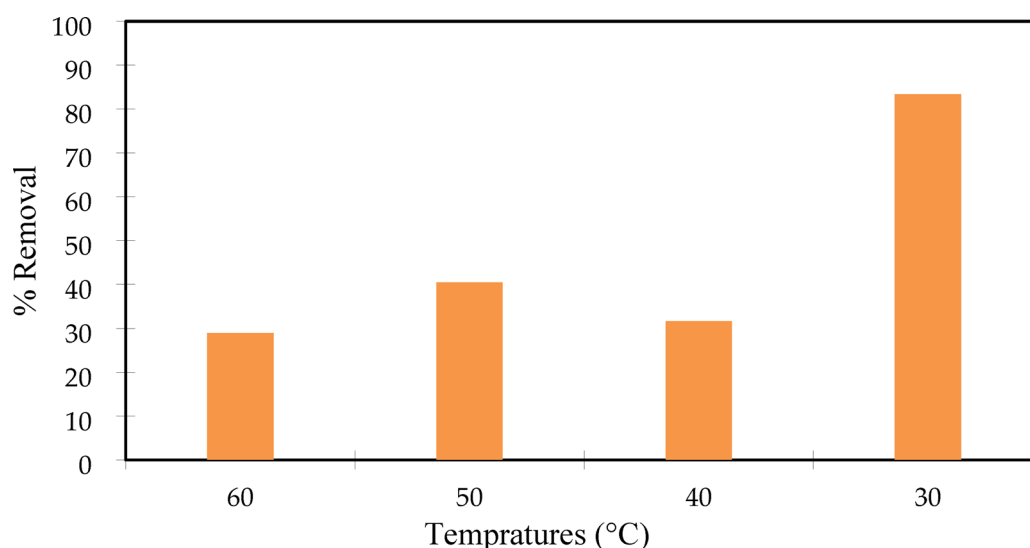


**Fig. 7.** Effect of temperature (°C) on AR73 dye onto a CFON.

Isotherm model	Isotherm parameter	Sunlight
Freundlich	$1/n$	2.208
	$K_f \text{ (mg}^{1-1/n} \text{L}^{1/n} \text{g}^{-1})$	64.410
	$R^2$	0.897
Langmuir	$Q_m \text{ (mg g}^{-1})$	322.58
	$K_a \times 10^3$	393.39
	$R^2$	0.461
Harkins-Jura isotherm	A	1.78
	B	1.00
	$R^2$	0.349

**Table 1.** Isotherm parameters of isotherm models for AR73 dye by CFON.

values of  $1/n$  (2.208) indicate favorable adsorption in conditions. A higher value in darkness suggests a more heterogeneous surface and potentially a wider distribution of adsorption energies<sup>76</sup>.

Additionally, the value of the factor “ $1/n$ ” in this study is greater than 1, indicating that using this isotherm equation to describe the chemical sorption mechanism on an external surface is preferable. Values of  $n > 1$  for dye particles indicate a heterogeneous nature of sorption and positive binding<sup>77</sup>. Chemisorption includes ion exchange, chelation, and complexation, while physisorption involves electrostatic interactions and van der Waals forces. Despite the higher  $K_f$  value (64.41), it is significantly higher in sunlight, indicating better adsorption efficiency under sunlight. The good fit of the Freundlich model ( $R^2 = 0.897$  in sunlight) suggests that it adequately describes the adsorption process and its heterogeneous nature (Supplementary Fig. 3). However, the Langmuir model assumes monolayer adsorption on a homogeneous surface. The data indicates a higher maximum adsorption capacity of  $322.58 \text{ mg g}^{-1}$  (Supplementary Fig. 4). This capacity is higher in dark conditions, suggesting that the adsorbent may have a stronger affinity for the dye in the absence of sunlight. The higher  $K_a$  value suggests a stronger affinity between AR73 and the nanocomposite. However, the lower  $R^2$  value of 0.461 for the Langmuir model compared to the Freundlich model indicates that it may not be the best fit for describing the adsorption process in this case. The Harkins-Jura model shows the poorest fit among the three models, with an  $R^2$  value of 0.349, indicating that it is not suitable for representing the adsorption process in this study (Supplementary Fig. 5). Table 1 displays A and B parameters, which are constants related to multilayer adsorption and the heat of adsorption, respectively. Both parameters are higher suggesting an enhanced adsorption capacity and energy. In this study, the Freundlich model demonstrates stronger correlation coefficients, indicating a better fit to the data compared to the Langmuir model. The Freundlich isotherm is found to be the most suitable for accurately describing the sorption equilibrium between AR73 dye and CFON nanoparticles with varying surface energies, confirming the heterogeneous nature of the adsorption process. The differences in parameters observed between light and dark conditions suggest that light may impact the adsorption process. The higher adsorption capacity and more heterogeneous surface observed in sunlight could be attributed to photocatalytic effects or light-induced changes in the adsorbent surface or dye molecules. Sunlight generally enhances adsorption capacity and intensity according to the Freundlich model. Previous studies have indicated that light can influence AR73 dye adsorption by promoting photocatalytic degradation or altering the surface properties of the adsorbent.

### Kinetic modeling of the adsorption process for AR73 dye removal

This study investigates the adsorption process of AR73 solution using chitosan/ferrous oxide nanocomposite. Kinetic models are employed to understand the rate of this reaction. Supplementary Table 5 summarizes the results obtained from fitting the experimental data to each kinetic model. The first-order model provides a simple approach for initial adsorption stages but might not capture the entire process. This model assumes the rate of adsorption is proportional to the concentration of the remaining dye molecules<sup>78</sup>. It describes a single-site adsorption process. The calculated  $q_e$  value ( $19.81 \text{ mg g}^{-1}$ ) deviates significantly from the experimental value, indicating a poor fit. The correlation coefficient ( $R^2$ ) of 0.897 suggests a moderate correlation, but not ideal for accurate representation (Fig. 8A). Pseudo-second-order model considers the rate of adsorption to be dependent on both the concentration of the dye and the available adsorption sites. It's often applied when the chemisorption process dominates. The calculated  $q_e$  ( $51.81 \text{ mg g}^{-1}$ ) shows a much closer match to the experimental value, implying a good fit. The  $R^2$  value of 0.999 indicates a strong positive correlation, suggesting the model effectively describes the adsorption process (Fig. 8B)<sup>79</sup>. The intraparticle diffusion model (Fig. 8C) focuses on the diffusion of dye molecules within the pores of the adsorbent material. It helps assess the contribution of diffusion to the overall rate-limiting step. It evaluates the role of diffusion within the adsorbent pores, but might not be the sole rate-limiting step. The  $R^2$  value of 0.76 signifies a weaker correlation compared to the second-order model. The constant  $K_{dif}$  (2.188) reflects the rate of intraparticle diffusion, but its importance might be limited in this case.

This deviation may be attributed to the difference in mass transfer rates between the initial and concluding phases of adsorption<sup>80</sup>. It's crucial to consult relevant research articles for a more comprehensive comparison. However, studies suggest that the pseudo-second-order model is often preferred for dye adsorption processes due to its ability to account for chemisorption and better represent the overall rate-limiting step. The values of constants ( $k_1$ ,  $k_2$ , and  $K_{dif}$ ) depend on various factors like initial dye concentration, adsorbent dosage, and solution temperature. An increase in these constants could indicate a faster adsorption rate, while a decrease

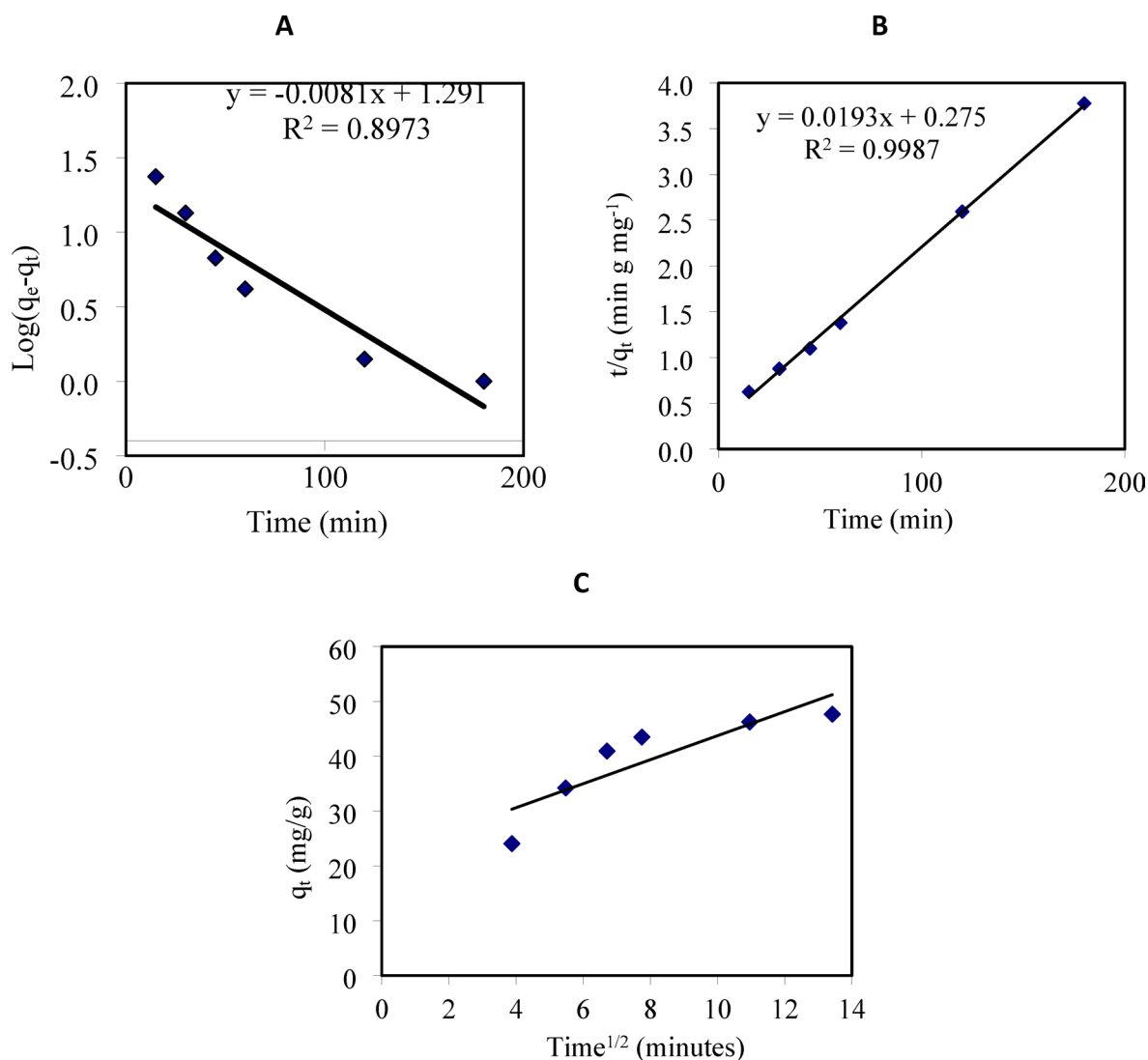


**Fig. 8.** First-order- kinetic model (A), second-order kinetic model (B), and interparticle diffusion kinetic model (C) for AR73 dye onto.

Water quality parameters	Values before treatment	Values after treatment	Increasing/decreasing percentages (%)
pH	7.34	7.46	1.63
DO (mg L <sup>-1</sup> )	4.46	4.42	-0.90
EC (μs Cm <sup>-1</sup> )	162	90	-44.44
TDS (mg L <sup>-1</sup> )	95	51	-46.32
Turbidity (NTV)	1220	1043	-14.51
NO <sub>3</sub> (μg L <sup>-1</sup> )	366.92	267.64	-27.06

**Table 2.** Influence of CFON treatment on several water quality parameters.

suggests a slower rate. Based on the results presented, the pseudo-second-order model appears to be the most suitable for describing the dye adsorption process. The high  $R^2$  value (0.999) indicates a strong correlation between the model and the experimental data. The calculated  $q_e$  value also closely matches the experimental value, suggesting good agreement.

#### Aquaculture water quality improvement

Table 2 shows the impact of CFON on water quality parameters of aquaculture effluent. The results reveal a positive influence of CFON on DO, EC, TDS, turbidity, and NO<sub>3</sub> values after treatment with CFON, compared to the same values before treatment. The results showed a slight increase in pH (from 7.34 to 7.46), which might

be attributed to the weak alkalinity of chitosan, a component of CFON. This minor shift is unlikely to pose a significant concern for most water applications<sup>81</sup>. A slight decrease in DO ( $4.46$  to  $4.42$  mg L<sup>-1</sup>) could be due to the adsorption of organic matter or oxygen consumption during potential Fenton-like reactions involving ferrous oxide nanoparticles<sup>82</sup>. Significant reductions in EC (from  $162$  to  $90$   $\mu$ S cm<sup>-1</sup>) and TDS (from  $95$  to  $51$  mg L<sup>-1</sup>) were reported, indicating the effectiveness of CFON in removing ionic contaminants. This result aligns with the specific adsorption properties of chitosan for various inorganic pollutants such as dyes and heavy metals<sup>83–85</sup>. The bioremediation of nitrogen sources from aquaculture effluents is a global concern<sup>86</sup>. In the current study, nitrate reduction (NO<sub>3</sub>) (from  $366.92$   $\mu$ g L<sup>-1</sup> to  $267.64$   $\mu$ g L<sup>-1</sup>) suggests potential adsorption or biodegradation processes facilitated by CFON. A notable decrease in turbidity (from  $1220$  NTU to  $1043$  NTU) signifies CFON's ability to aggregate and remove suspended particles. This could be due to electrostatic interactions between the charged surfaces of CFON and the particles, or bridging mechanisms involving the chitosan component. This finding was previously reported by several studies suggesting that CFON may remove the dissolved salts<sup>87–89</sup>.

Chitosan has shown promise in nitrate removal through adsorption and ion exchange. Additionally, the nanocomposite might create microenvironments suitable for denitrifying bacteria to flourish and contribute to biological nitrate reduction. The synergistic action of chitosan and ferrous oxide in CFON contributes to its water treatment efficacy, chitosan offers abundant functional groups for electrostatic adsorption of ionic contaminants and complexation with organic pollutants<sup>90</sup>. Its porous structure facilitates physical adsorption as well. While ferrous oxide provides additional adsorption sites for specific pollutants and potentially initiates Fenton-like reactions for the degradation of organic matter<sup>91</sup>.

### Comparative study of acid red 73 adsorption capacities

Supplementary Table 6 presents a comparative analysis of different adsorbents utilized for the removal of Acid Red 73 dye from wastewater. The range of materials reviewed reflects various adsorption strategies, from natural biomass to advanced nanocomposites.

Bio-based adsorbents such as chitosan, rice wine lees, and acid-treated water hyacinth stems offer environmentally friendly and cost-effective options. However, these materials generally exhibit moderate adsorption capacities— $18.74$  mg/g for rice wine lees and  $50$  mg/g for acid-treated water hyacinth stems<sup>92,93</sup>. Nanoparticles, including Fe<sub>3</sub>O<sub>4</sub> and chitosan-based nanomaterials, have been explored for their high surface area and reactivity. Yet, their adsorption performances remain limited, with Fe<sub>3</sub>O<sub>4</sub> nanoparticles achieving  $40.1$  mg/g and chitosan nanoparticles only  $1.25$  mg/g<sup>80,94</sup> possibly due to challenges in synthesis, dispersion, or surface functionalization.

Engineered hydrogels, such as carbon nanotube/chitosan and lignin-based hydrogels, show improved capacities ( $24.73$  mg/g and  $47.59$  mg/g, respectively)<sup>95,96</sup> reflecting the growing sophistication in polymer design for dye adsorption. Remarkably, the chitosan/ferrous oxide nanocomposite developed in this study exhibited a significantly higher adsorption capacity of  $322.58$  mg/g, far surpassing all other materials listed<sup>97</sup>. This exceptional performance (This study) suggests a strong synergistic effect between the chitosan matrix and the embedded iron oxide nanoparticles, which likely enhances the density of active adsorption sites and improves affinity toward Acid Red 73.

### Regeneration and reusability of the sorbent material

Evaluating the regeneration and reusability of adsorbent materials is a key factor in determining their practicality and cost-effectiveness for environmental applications such as wastewater treatment<sup>98</sup>. In the current study, the reusability of the composite was assessed through successive adsorption-desorption cycles using a  $50$  mg/L solution of Acid Red 73 dye. The experimental conditions involved agitation at  $180$  rpm for  $4$  h, simulating realistic operational parameters (Fig. 9).

During the initial adsorption cycle (R1), the composite exhibited excellent performance, achieving a dye removal efficiency of  $98.160\%$ , indicating strong binding affinity between the adsorbent surface and dye molecules. In the second cycle (R2), a moderate reduction in performance was observed, with the efficiency decreasing to  $88.7\%$ . Despite this decline, the composite still maintained a considerable removal capacity, reflecting its structural stability and reusability.

However, a pronounced drop in adsorption efficiency was recorded in the third cycle (R3), where removal efficiency fell sharply to  $9.99\%$ . This significant reduction suggests a marked deterioration in the adsorbent's active sites or surface functionality after repeated use. While the composite demonstrated promising reusability over the first two cycles, the third cycle revealed limitations that may be linked to saturation of adsorption sites, structural fatigue, or potential chemical alterations on the surface. These findings emphasize that although the composite is initially effective and partially reusable, its long-term application may require regeneration strategies or material reinforcement to sustain high performance. The decline observed in later cycles should be taken into account when considering its deployment in continuous or large-scale treatment systems.

### Conclusion

The chitosan/ferrous oxide nanocomposite (CFON) demonstrated exceptional performance in removing Acid Red 73 dye (AR73) from aqueous solutions, exhibiting high adsorption capacity and photocatalytic activity under sunlight irradiation achieving a maximum removal percentage of  $99.3\%$ . The nanocomposite's efficacy was confirmed through comprehensive characterization and batch adsorption experiments, revealing the influence of various parameters on dye removal efficiency. The adsorption process was found to be exothermic, spontaneous, and best described by the Freundlich isotherm model, while the kinetic studies indicated a pseudo-second-order model, suggesting chemisorption as the dominant mechanism. The synergistic effect of adsorption and photocatalytic degradation under sunlight resulted in significant dye removal. As well as, the results concluded that the CFON has positive impacts on water quality parameters of aquaculture effluent. CFON has improved



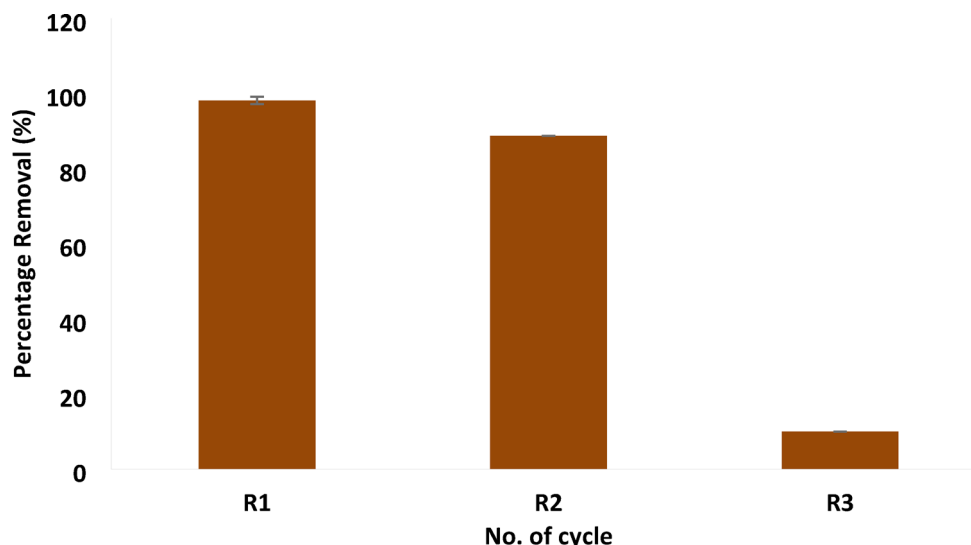


**Fig. 9.** Reusability study of acid red 73 dye.

the water quality parameters of aquaculture effluent wastewater. The pH was slightly increased. While reducing the values of EC (44.4%), TDS (46.3%), turbidity (14%), and  $\text{NO}_3$  (27%). These findings highlight the promising potential of CFON as a sustainable and efficient solution for removing hazardous dyes and improving water quality in various applications.

### Data availability

The datasets used and/or analyzed during the current study are available from the corresponding author upon reasonable request.

Received: 15 March 2025; Accepted: 26 May 2025

Published online: 02 July 2025

### References

- Zhang, Y. & Zhang, J. Surface modification of monodisperse magnetite nanoparticles for improved intracellular uptake to breast cancer cells. *J. Colloid Interface Sci.* **283**, 352–357 (2005).
- Alprol, A. E., Mansour, A. T., Abdelwahab, A. M. & Ashour, M. Advances in green synthesis of metal oxide nanoparticles by marine algae for wastewater treatment by adsorption and photocatalysis techniques. *Catalysts* **13**, 888 (2023).
- Dawood, M. A. et al. Selenium nanoparticles as a natural antioxidant and metabolic regulator in aquaculture: a review. *Antioxidants* **10**, 1364 (2021).
- Kluchova, K. et al. Superparamagnetic maghemite nanoparticles from solid-state synthesis—Their functionalization towards peroral MRI contrast agent and magnetic carrier for trypsin immobilization. *Biomaterials* **30**, 2855–2863 (2009).
- Monteserín, M., Larumbe, S., Martínez, A. V. & Burgui, S. Francisco martin, L. Recent advances in the development of magnetic nanoparticles for biomedical applications. *J. Nanosci. Nanotechnol.* **21**, 2705–2741 (2021).
- Baabu, P. R. S. et al. B. Iron oxide nanoparticles: a review on the Province of its compounds, properties and biological applications. *Materials* **16**, 59 (2022).
- Abbas, E. M., Al-Souti, A. S., Sharawy, Z. Z., El-Haroun, E. & Ashour, M. Impact of dietary administration of seaweed polysaccharide on growth, microbial abundance, and growth and immune-related genes expression of the Pacific whiteleg shrimp (*Litopenaeus vannamei*). *Life* **13**, 344 (2023).
- Schubert, J. & Chanana, M. Coating matters: review on colloidal stability of nanoparticles with biocompatible coatings in biological media, living cells and organisms. *Curr. Med. Chem.* **25**, 4553–4586 (2018).
- Iber, B. T., Kasan, N. A., Torsabo, D. & Omuwa, J. W. A review of various sources of Chitin and Chitosan in nature. *J. Renew. Mater.* **10**, 1097 (2022).
- Narmani, A. & Jafari, S. M. Chitosan-based nanodelivery systems for cancer therapy: recent advances. *Carbohydr. Polym.* **272**, 118464 (2021).
- Patel, M. P., Patel, R. R. & Patel, J. K. Chitosan mediated targeted drug delivery system: a review. *J. Pharm. Pharm. Sci.* **13**, 536–557 (2010).
- Yan, D. et al. Antimicrobial properties of Chitosan and Chitosan derivatives in the treatment of enteric infections. *Molecules* **26**, 7136 (2021).
- Abu-Elala, N. M., Hossam-Elden, N. & Marzouk, M. S. & El Basuini, M. F. Chitosan for Aquaculture: Growth Promotion, Immune Modulation, Antimicrobial Activity, bio-carrier Utility, Water Quality Management, and Safety Considerations. *Ann. Anim. Sci.*
- Nehra, P., Chauhan, R., Garg, N. & Verma, K. Antibacterial and antifungal activity of Chitosan coated iron oxide nanoparticles. *Br. J. Biomed. Sci.* **75**, 13–18 (2018).
- Vigneshwaran, S., Sirajudheen, P. & Meenakshi, S. Surface activated mesoporous Ag-Fe<sub>3</sub>O<sub>4</sub> tethered Chitosan nanomatrix heterojunction photocatalyst for organic dyes degradation: performance, recycling, and mechanism. *Environ. Nanotechnol. Monit. Manage.* **17**, 100654 (2022).
- Wang, C. & Chakrapani, V. Photocatalytic generation of reactive oxygen species on Fe and Mn oxide minerals: mechanistic pathways and influence of semiconducting properties. *J. Phys. Chem. C.* **127**, 23189–23198 (2023).
- Dai, Y. et al. Reactive oxygen species-scavenging nanomaterials for the prevention and treatment of age-related diseases. *J. Nanobiotechnol.* **22** (2024).

18. Farhan, A. et al. Metal ferrites-based nanocomposites and nanohybrids for photocatalytic water treatment and electrocatalytic water splitting. *Chemosphere* **310**, 136835 (2023).
19. Kumar, N., Gusain, R., Pandey, S. & Ray, S. S. Hydrogel nanocomposite adsorbents and photocatalysts for sustainable water purification. *Adv. Mater. Interfaces* **10**, 2201375 (2023).
20. Mehmood, A. et al. Magnetic nanocomposites for sustainable water purification—a comprehensive review. *Environ. Sci. Pollut. Res.* **28**, 19563–19588 (2021).
21. Alprol, A. E., Mansour, A. T., Ibrahim, M. E. E. & Ashour, M. Artificial intelligence technologies revolutionizing wastewater treatment: current trends and future prospective. *Water* **16**, 314. <https://doi.org/10.3390/w16020314> (2024).
22. Madhav, S. et al. Water pollutants: sources and impact on the environment and human health. *Sensors Water Pollutants Monitoring: Role Material*, 43–62 (2020).
23. Mansour, A. T., Ashour, M., Alprol, A. E. & Alsaqufi, A. S. Aquatic plants and aquatic animals in the context of sustainability: cultivation techniques, integration, and blue revolution. *Sustainability* **14**, 3257 (2022).
24. Rath, B. S., Kumar, P. S. & Vo, D. V. N. Critical review on hazardous pollutants in water environment: occurrence, monitoring, fate, removal technologies and risk assessment. *Sci. Total Environ.* **797**, 149134 (2021).
25. Feng, Y. et al. Basic dye adsorption onto an agro-based waste material—Sesame hull (*Sesamum indicum* L.). *Bioresour. Technol.* **102**, 10280–10285 (2011).
26. Abdallah, M. A. M. & Alprol, A. E. Utilization of aquatic biomass as biosorbent for sustainable production of high surface area, nano-microporous, for removing two dyes from wastewater. *Sci. Rep.* **14**, 4471 (2024).
27. Alprol, A. Study of environmental concerns of dyes and recent textile effluents treatment technology: a review. *Asian J. Fish. Aquat. Res.* **3**, 1–18 (2019).
28. Alprol, A. E. et al. Potential applications of *Arthrospira platensis* Lipid-Free biomass in bioremediation of organic dye from industrial textile effluents and its influence on marine rotifer (*Brachionus plicatilis*). *Mater. (Basel)* **14**. <https://doi.org/10.3390/ma14164446> (2021).
29. Alprol, A. E., Khedawy, M., Ashour, M. & Thabet, W. M. *Arthrospira platensis* nanoparticle-based approach for efficient removal of Methyl orange dye from aqueous solutions: isotherm, kinetic, and thermodynamic analysis. *Biomass Convers. Biorefinery*. 1–15. <https://doi.org/10.1007/s13399-023-04844-z>. (2023).
30. Thabet, W. M., Alprol, A. E., Ashour, M., Khedawy, M. & Esraa, A. E. Response surface methodology application in optimization of oily wastewater treatment by *Sargassum latifolium*. *Egypt. J. Aquat. Biology Fisheries* **28**, 1639–1658 (2024).
31. Gupta, V. Application of low-cost adsorbents for dye removal—a review. *J. Environ. Manage.* **90**, 2313–2342 (2009).
32. Ghoneim, M. M. et al. Removal of cadmium from aqueous solution using marine green algae, *Ulva lactuca*. *Egypt. J. Aquat. Res.* **40**, 235–242 (2014).
33. Ashour, M. et al. Ammonia bioremediation from aquaculture wastewater effluents using *Arthrospira platensis* NIOF17/003: impact of biodiesel residue and potential of ammonia-loaded biomass as rotifer feed. *Materials* **14**, 5460 (2021).
34. El Basuini, M. F. et al. Impacts of algae supplements (*Arthrospira* & *Chlorella*) on growth, nutrient variables, intestinal efficacy, and antioxidants in new Zealand white rabbits. *Sci. Rep.* **13**, 7891 (2023).
35. Sallam, G. R., Habib, Y. J., Basuini, E., Fayed, M. F., Shehata, A. I. & W. M. & Synergistic interactions of zeolite, stocking density, and water exchange: A holistic approach to optimizing aquaculture performance of juvenile European Seabass (*Dicentrarchus labrax*). *Sci. Afr.* **23**, e02043 (2024).
36. Bashir, I. et al. Concerns and threats of contamination on aquatic ecosystems. *Bioremediation Biotechnology: Sustainable Approaches Pollution Degradation*, 1–26 (2020).
37. Sarode, S. et al. Overview of wastewater treatment methods with special focus on biopolymer chitin-chitosan. *Int. J. Biol. Macromol.* **121**, 1086–1100 (2019).
38. Karim, A. V., Krishnan, S., Pisharody, L., Malhotra, M. & Bustillo-Lecompte, C. Application of ferrate for advanced water and wastewater treatment. *Adv. Oxid. Process.* **5**, 79 (2020).
39. Munyengabe, A. & Zvinowanda, C. Production, characterization and application of ferrate (VI) in water and wastewater treatments. *Braz J. Anal. Chem.* **6**, 40–57 (2019).
40. Gozdecka, A. & Wiącek, A. E. Effect of UV radiation and Chitosan coating on the adsorption-photocatalytic activity of TiO<sub>2</sub> particles. *Mater. Sci. Eng. C* **93**, 582–594 (2018).
41. Bui, V. K. H., Park, D. & Lee, Y. C. Chitosan combined with ZnO, TiO<sub>2</sub> and Ag nanoparticles for antimicrobial wound healing applications: a mini review of the research trends. *Polymers* **9**, 21 (2017).
42. Quy, B. et al. Photocatalytic degradation performance of a chitosan/ZnO-Fe<sub>3</sub>O<sub>4</sub> nanocomposite over cationic and anionic dyes under visible-light irradiation. *RSC Adv.* **15**, 1590–1603 (2025).
43. Antony Arockiaraj, M., Mani, G. & AlOthman, Z. A. Effect of chitosan-incorporated Fe<sub>3</sub>O<sub>4</sub> nanocomposites on the photocatalytic removal of organic molecules. *J. Mater. Sci.: Mater. Electron.* **33**, 9570–9579 (2022).
44. Qomariyah, L. et al. Synergistic photocatalytic and adsorption capabilities of ZnO/chitosan/cmc for organic dye degradation under sunlight irradiation. *Int. J. Biol. Macromol.* **305**, 141134 (2025).
45. Preethi, S. et al. Synthesis and characterization of chitosan/zinc oxide nanocomposite for antibacterial activity onto cotton fabrics and dye degradation applications. *Int. J. Biol. Macromol.* **164**, 2779–2787 (2020).
46. Al-Ghouti, M. A. & Al-Absi, R. S. Mechanistic Understanding of the adsorption and thermodynamic aspects of cationic methylene blue dye onto cellulosic Olive stones biomass from wastewater. *Sci. Rep.* **10**, 15928 (2020).
47. EPA, U. National recommended water quality criteria EPA-822-R-02-047. *Office Sci. Technol.* (2002).
48. Júnior, J. A. A. & Baldo, J. B. The behavior of zeta potential of silica suspensions. *New J. Glass Ceram.* **4**, 29 (2014).
49. Forest, V. & Pourchez, J. Preferential binding of positive nanoparticles on cell membranes is due to electrostatic interactions: A too simplistic explanation that does not take into account the nanoparticle protein Corona. *Mater. Sci. Eng. C* **70**, 889–896 (2017).
50. Dakhil, I. H. A comparative study for removal of dyes from textile effluents by low cost adsorbents. *Mesopotamia Env J. Special Issue A*, 1–9 (2016).
51. Gupta, V., Agarwal, A., Singh, M. & Singh, N. Removal of red RB dye from aqueous solution by Belpatra bark charcoal (BBC) adsorbent. *J. Mater. Environ. Sci.* **8**, 3654–3665 (2017).
52. Yu, J. G. et al. Graphene nanosheets as novel adsorbents in adsorption, preconcentration and removal of gases, organic compounds and metal ions. *Sci. Total Environ.* **502**, 70–79 (2015).
53. Azizi, S., Mahdavi Shahri, M. & Mohamad, R. Green synthesis of zinc oxide nanoparticles for enhanced adsorption of lead ions from aqueous solutions: equilibrium, kinetic and thermodynamic studies. *Molecules* **22**, 831 (2017).
54. Abate, G. Y., Alene, A. N., Habte, A. T. & Getahun, D. M. Adsorptive removal of malachite green dye from aqueous solution onto activated carbon of *Catha edulis* stem as a low cost bio-adsorbent. *Environ. Syst. Res.* **9**, 1–13 (2020).
55. Peng, X. et al. Adsorption of 1, 2-dichlorobenzene from water to carbon nanotubes. *Chem. Phys. Lett.* **376**, 154–158 (2003).
56. Fouda, A. et al. -D. Phyco-synthesized zinc oxide nanoparticles using marine macroalgae, *Ulva fasciata* delile, characterization, antibacterial activity, photocatalysis, and tanning wastewater treatment. *Catalysts* **12**, 756 (2022).
57. Mussa, Z. H., Al-Qaim, F. F., Yuzir, A. & Shameli, K. Photocatalytic removal of malachite green and brilliant blue dyes from its aqueous solution: A case study of factorial experimental design. *J. Mex. Chem. Soc.* **65**, 247–255 (2021).
58. Hamza, M. F. et al. Photocatalytic efficacy of heterocyclic base grafted Chitosan magnetite nanoparticles on sorption of Pb (II); application on mining effluent. *Catalysts* **12**, 330 (2022).

59. Klubnuan, S., Suwanboon, S. & Amornpitoksuk, P. Effects of optical band gap energy, band tail energy and particle shape on photocatalytic activities of different ZnO nanostructures prepared by a hydrothermal method. *Opt. Mater.* **53**, 134–141 (2016).
60. Fouda, A., Hassan, S. E. D., Saied, E. & Hamza, M. F. Photocatalytic degradation of real textile and tannery effluent using biosynthesized magnesium oxide nanoparticles (MgO-NPs), heavy metal adsorption, phytotoxicity, and antimicrobial activity. *J. Environ. Chem. Eng.* **9**, 105346 (2021).
61. Mansour, A. T. et al. The using of nanoparticles of microalgae in remediation of toxic dye from industrial wastewater: kinetic and isotherm studies. *Mater. (Basel)*. **15**. <https://doi.org/10.3390/ma15113922> (2022).
62. Xiao, X. H., Chen, X. X., Xu, T. T. & Li, X. J. High-efficiency visible photocatalytic degradation of Methyl orange by silicon nanoporous pillar array. *Mater. Lett.* **211**, 96–99 (2018).
63. Dutta, M., Basu, J. K., Faraz, M. H., Gautam, N. & Kumar, A. Fixed-bed column study of textile dye direct blue 86 by using a composite adsorbent. *Archives Appl. Sci. Res.* **4**, 882–891 (2012).
64. Markovska, L., Meshko, V. & Noveski, V. Adsorption of basic dyes in a fixed bed column. *Korean J. Chem. Eng.* **18**, 190–195 (2001).
65. Al-Sultani Kadhim, F. & Al-Seroury, F. Characterization the removal of phenol from aqueous solution in fluidized bed column by rice husk adsorbent. *Res. J. Recent. Sci. ISSN.* **2277**, 2502 (2012).
66. Zheng, Q., Shen, H. & Shuai, D. Emerging investigators series: advances and challenges of graphitic carbon nitride as a visible-light-responsive photocatalyst for sustainable water purification. *Environ. Science: Water Res. Technol.* **3**, 982–1001 (2017).
67. Vijai Anand, K. et al. Photocatalytic degradation of Rhodamine B dye using biogenic hybrid ZnO-MgO nanocomposites under visible light. *ChemistrySelect* **4**, 5178–5184 (2019).
68. Galushchinskiy, A., González-Gómez, R., McCarthy, K., Farràs, P. & Savateev, A. Progress in development of photocatalytic processes for synthesis of fuels and organic compounds under outdoor solar light. *Energy Fuels*. **36**, 4625–4639 (2022).
69. Tahir, D. et al. Enhanced visible-light absorption of Fe<sub>2</sub>O<sub>3</sub> covered by activated carbon for multifunctional purposes: tuning the structural, electronic, optical, and magnetic properties. *ACS Omega*. **6**, 28334–28346 (2021).
70. Babarinde, N. A., Oyesiku, O. & Dairo, O. F. Isotherm and thermodynamic studies of the biosorption of copper (II) ions by erythrodontium Barteri. *Int. J. Phys. Sci.* **2**, 300–304 (2007).
71. Wang, H., Luo, W., Guo, R., Li, D. & Xue, B. Effective adsorption of congo red dye by magnetic Chitosan prepared by solvent-free ball milling. *Mater. Chem. Phys.* **292**, 126857 (2022).
72. Abualnaja, K. M., Alprol, A. E., Ashour, M. & Mansour, A. T. Influencing multi-walled carbon nanotubes for the removal of ismate Violet 2R dye from wastewater: isotherm, kinetics, and thermodynamic studies. *Appl. Sci.* **11**, 4786 (2021).
73. Freundlich, H. M. F. Over the adsorption in solution. *J. Phys. Chem.* **57**, 1100–1107 (1906).
74. Langmuir, I. The constitution and fundamental properties of solids and liquids. Part I. Solids. *J. Am. Chem. Soc.* **38**, 2221–2295 (1916).
75. Harkins, W. D. & Jura, G. An adsorption method for the determination of the area of a solid without the assumption of a molecular area, and the area occupied by nitrogen molecules on the surfaces of solids. *J. Chem. Phys.* **11**, 431–432 (1943).
76. Salazar-Rabago, J. J., Leyva-Ramos, R., Rivera-Utrilla, J., Ocampo-Perez, R. & Cerino-Cordova, F. J. Biosorption mechanism of methylene blue from aqueous solution onto white pine (*Pinus durangensis*) sawdust: effect of operating conditions. *Sustainable Environ. Res.* **27**, 32–40 (2017).
77. Raval, N. P., Shah, P. U. & Shah, N. K. Malachite green a cationic dye and its removal from aqueous solution by adsorption. *Appl. Water Sci.* **7**, 3407–3445 (2017).
78. Volesky, B. Biosorption and me. *Water Res.* **41**, 4017–4029 (2007).
79. Sen, T. K. & Sarzali, M. V. Removal of cadmium metal ion (Cd<sup>2+</sup>) from its aqueous solution by aluminium oxide (Al<sub>2</sub>O<sub>3</sub>): A kinetic and equilibrium study. *Chem. Eng. J.* **142**, 256–262 (2008).
80. Liu, Q. S., Zheng, T., Wang, P., Jiang, J. P. & Li, N. Adsorption isotherm, kinetic and mechanism studies of some substituted phenols on activated carbon fibers. *Chem. Eng. J.* **157**, 348–356 (2010).
81. Waheed, S. & Khan, G. R. Toxicity of dyes and dye intermediates. *Biol. Sciences-PJSIR*. **47**, 76–90 (2004).
82. Ebrahimi, E. E., Al-Maghrabi, M. N. & Mobarki, A. R. Removal of organic pollutants from industrial wastewater by applying photo-Fenton oxidation technology. *Arab. J. Chem.* **10**, S1674–S1679 (2017).
83. Sirajudheen, P., Poovathumkuzhi, N. C., Vigneshwaran, S., Chelaveetil, B. M. & Meenakshi, S. Applications of Chitin and Chitosan based biomaterials for the adsorptive removal of textile dyes from water—A comprehensive review. *Carbohydr. Polym.* **273**, 118604 (2021).
84. Kausar, A. et al. Chitosan-cellulose composite for the adsorptive removal of anionic dyes: experimental and theoretical approach. *J. Mol. Liq.* **391**, 123347 (2023).
85. Zia, Q., Tabassum, M., Gong, H. & Li, J. A review on Chitosan for the removal of heavy metals ions. *J. Fiber Bioeng. Inf.* **12**, 103–128 (2019).
86. Ashour, M. et al. M.-A. A liquid seaweed extract (TAM<sup>®</sup>) improves aqueous rearing environment, diversity of zooplankton community, whilst enhancing growth and immune response of Nile tilapia, *Oreochromis niloticus*, challenged by *Aeromonas hydrophila*. *Aquaculture* **543**, 736915 (2021).
87. Keshvardoostchokami, M., Babaei, L., Zamani, A., Parizanganeh, A. & Piri, F. Synthesized chitosan/iron oxide nanocomposite and shrimp shell in removal of nickel, cadmium and lead from aqueous solution. (2017).
88. Park, J. E. et al. Removal of hexavalent chromium (VI) from wastewater using chitosan-coated iron oxide nanocomposite membranes. *Toxics* **10**, 98 (2022).
89. Gerard, N., Krishnan, R. S., Ponnusamy, S. K., Cabana, H. & Vaidyanathan, V. K. Adsorptive potential of dispersible Chitosan coated iron-oxide nanocomposites toward the elimination of arsenic from aqueous solution. *Process Saf. Environ. Prot.* **104**, 185–195 (2016).
90. Xia WenShui, X. W., Liu Ping, L. P. & Zhang JiaLi, Z. J. & Chen jie, C. J. Biological activities of Chitosan and chitoooligosaccharides. (2010).
91. Aziz, T., Masum, S., Qadir, M., Gafur, A. & Huq, D. Physicochemical characterization of iron oxide nanoparticle coated with Chitosan for biomedical application. *Int. Res. J. Pure Appl. Chem.* **11**, 1–9 (2016).
92. Wang, Q. et al. Adsorption of Azo Dye Acid Red 73 onto rice wine lees: adsorption kinetics and isotherms. *Adv. Mater. Sci. Eng.* **3469579** (2020).
93. El-Adawy, H. A. Kinetics and thermodynamic study of acid red 73 dye removal on HCl-water hyacinth stems biomass. *Egypt. J. Chem.* **63**, 1555–1566 (2020).
94. Cheung, W., Szeto, Y. & McKay, G. Enhancing the adsorption capacities of acid dyes by Chitosan nano particles. *Bioresour. Technol.* **100**, 1143–1148 (2009).
95. Shuxia, W., Wu, C., Zhiming, T., Jiang, N. & Mijia, Z. Synthesis of a functional biomass lignin-based hydrogel with high swelling and adsorption capability towards acid red 73. *Environ. Sci. Pollut. Res.* **28**, 51306–51320 (2021).
96. Wei, J. et al. Carbon nanotube/chitosan hydrogel for adsorption of acid red 73 in aqueous and soil environments. *BMC Chem.* **17**, 104 (2023).
97. Jia, W. et al. Infrared imaging of modified Chitosan hydrogel film morphology study of Polyvinyl alcohol adsorption. *Multimedia Tools Appl.* **79**, 17027–17043 (2020).
98. Fouda-Mbanga, B. G., Onotu, O. & Tywabi-Ngeva, Z. Advantages of the reuse of spent adsorbents and potential applications in environmental remediation: A review. *Green Anal. Chemistry*, 100156 (2024).

## Acknowledgements

The authors express their gratitude to the support of Princess Nourah bint Abdulrahman University Researchers Supporting Project number (PNURSP2025R58), Princess Nourah bint Abdulrahman University, Riyadh, Saudi Arabia, and Deanship of Scientific Research, Vice Presidency for Graduate Studies and Scientific Research, King Faisal University, Saudi Arabia (KFU242245).

## Author contributions

AEA: Conceptualization, Methodology, investigation, Software, Formal analysis, Writing—review and editing, Writing—original draft preparation, Project administration. AB: Conceptualization, Investigation, Validation, Resources, Writing—review and editing. SIAI: Writing—review and editing, Funding acquisition, Visualization, Investigation. ATM: Writing—review and editing, Funding acquisition, Visualization, Investigation. EEL-H: Writing—review and editing, Funding acquisition, Visualization, Investigation. MNA: Writing—review and editing, Funding acquisition, Visualization, Investigation. MA: Conceptualization, Software, Writing—review and editing, Writing—original draft preparation, Visualization, Investigation.

## Funding

The authors express their gratitude to the support of Princess Nourah bint Abdulrahman University Researchers Supporting Project number (PNURSP2025R58), Princess Nourah bint Abdulrahman University, Riyadh, Saudi Arabia, and Deanship of Scientific Research, Vice Presidency for Graduate Studies and Scientific Research, King Faisal University, Saudi Arabia (KFU242245).

## Declarations

## Competing interests

The authors declare no competing interests.

## Additional information

**Supplementary Information** The online version contains supplementary material available at <https://doi.org/10.1038/s41598-025-04207-w>.

**Correspondence** and requests for materials should be addressed to A.T.M., E.E.-H. or M.A.

**Reprints and permissions information** is available at [www.nature.com/reprints](http://www.nature.com/reprints).

**Publisher's note** Springer Nature remains neutral with regard to jurisdictional claims in published maps and institutional affiliations.

**Open Access** This article is licensed under a Creative Commons Attribution-NonCommercial-NoDerivatives 4.0 International License, which permits any non-commercial use, sharing, distribution and reproduction in any medium or format, as long as you give appropriate credit to the original author(s) and the source, provide a link to the Creative Commons licence, and indicate if you modified the licensed material. You do not have permission under this licence to share adapted material derived from this article or parts of it. The images or other third party material in this article are included in the article's Creative Commons licence, unless indicated otherwise in a credit line to the material. If material is not included in the article's Creative Commons licence and your intended use is not permitted by statutory regulation or exceeds the permitted use, you will need to obtain permission directly from the copyright holder. To view a copy of this licence, visit <http://creativecommons.org/licenses/by-nc-nd/4.0/>.

© The Author(s) 2025